



## ORIGINAL ARTICLE

# Preparation of *Quercus mongolica* leaf-derived porous carbon with a large specific surface area for highly effective removal of dye and antibiotic from water



Qinghua Zhou<sup>a,c,1</sup>, Yingying Wu<sup>a,d,1</sup>, Huanjia Chen<sup>a</sup>, Guanya Zhu<sup>a</sup>,  
Yupeng Zhang<sup>a</sup>, Dadong Liang<sup>a,b,\*</sup>, Guang Chen<sup>b</sup>, Shanshan Tang<sup>b,\*</sup>

<sup>a</sup> College of Resource and Environment, Jilin Agricultural University, Changchun 130118, China

<sup>b</sup> Key Laboratory of Straw Comprehensive Utilization and Black Soil Conservation, The Ministry of Education, College of Life, Jilin Agricultural University, Changchun, Jilin 130118, China

<sup>c</sup> College of Resources, Sichuan Agricultural University, Chengdu 611130, China

<sup>d</sup> College of Plant Protection, Nanjing Agricultural University, Nanjing 210095, China

Received 26 March 2022; accepted 5 June 2022

Available online 8 June 2022

## KEYWORDS

*Quercus mongolica* leaf;  
Porous carbon;  
Adsorption;  
Dye;  
Antibiotic

**Abstract** *Quercus mongolica* leaf (QL), an easily available biomass, was used as the precursor for preparing the hierarchical porous carbon with a large specific surface area and high adsorption capacities toward the representative dye and antibiotic. After being carbonized, QL was further chemically activated, and potassium hydroxide was proved to be a better activator than sodium hydroxide. The QL-derived porous carbon (PCQL) exhibited abundant micro- and mesopores, and the specific surface area reached 3275 m<sup>2</sup> g<sup>-1</sup>. The performances of PCQL were evaluated through adsorbing rhodamine B (RhB) and tetracycline hydrochloride (TC) from water. Four adsorption isotherm models (the Langmuir, Freundlich, Sips, and Redlich-Peterson models), three adsorption kinetic models (the pseudo-first-order, pseudo-second-order, and intra-particle diffusion models), and the thermodynamic equations were used to investigate the adsorption processes. The pseudo-second-order kinetic model and the Sips isotherm model fitted the experimental data well, which indicates that the adsorption processes were controlled by the amount of adsorption active sites on the surface of PCQL, and these adsorption active sites had different affinities for the adsorbates. The maximum adsorption capacities of PCQL toward RhB and TC were 1946.0 and

\* Corresponding authors at: College of Resource and Environment, Jilin Agricultural University, Changchun 130118, China (D. Liang).

E-mail addresses: [liangdadong@jlau.edu.cn](mailto:liangdadong@jlau.edu.cn) (D. Liang), [tangshanshan81@163.com](mailto:tangshanshan81@163.com) (S. Tang).

<sup>1</sup> These authors contributed equally to this work.

Peer review under responsibility of King Saud University.



1479.6 mg g<sup>-1</sup>, respectively, based on the Sips model. The thermodynamic analysis indicates that the adsorption of PCQL toward adsorbents was spontaneous physical processes accompanied by the increasing disorder degree. The adsorption mechanism was attributed to the combination of the pore-filling, hydrogen bond, and  $\pi$ - $\pi$  interactions. Moreover, in the fixed-bed experiments, the Yoon-Nelson model fitted the breakthrough curves well, and about 8 L wastewater containing RhB (200 mg L<sup>-1</sup>) may be effectively treated by 1.0 g of PCQL. Above results indicate that QL is a promising precursor for preparing functional porous carbon materials.

© 2022 The Author(s). Published by Elsevier B.V. on behalf of King Saud University. This is an open access article under the CC BY-NC-ND license (<http://creativecommons.org/licenses/by-nc-nd/4.0/>).

## 1. Introduction

Water is an essential but limited resource. Unfortunately, large volumes of water have been contaminated by various industrial and agricultural effluents, which brings huge potential hazard to the environment. For example, as one of the most important dyes, rhodamine B (RhB) has been extensively used as the colorant in the textile, leather, and paint industries and the biological stain in the biomedical laboratories. RhB is toxic and carcinogenic, and may irritate the eyes, skin, and respiratory system. Thus, the presence of RhB in water is potentially hazardous toward humans and animals (Huang et al., 2016; Liu et al., 2015). Moreover, tetracycline (TC) is one of the antibiotics which have been extensively used in the livestock and aquaculture industries and human therapy. However, only a small fraction of TC may be metabolized and adsorbed by humans and animals, and most of them are finally excreted into the environment such as domestic sewage, aquaculture wastewater, medical wastewater, and soil. The existence of TC in aquatic environment may bring negative effect on plant growth, human health, and microbial community structure, and accelerate the occurrence of antibiotic resistance genes (Gao et al., 2012; Qiao et al., 2020; Babaei et al., 2016).

At present, various chemical, biological, and physical methods have been utilized for removal of the threatening pollutants from aqueous media, including adsorption, advanced oxidation processes, chemical precipitation, ultrafiltration, microbial degradation, and so on (Dong et al., 2022; Gadipelly et al., 2014; Zhao et al., 2018). Among the methods of wastewater treatment, adsorption is especially promising because of the advantages such as high efficiency, low cost, ease of operation, and simplicity (Abd El-Monaem et al., 2022; Omer et al., 2022). The advantages of adsorption are closely related to the utilization of adsorbents. Therefore, many efforts have been devoted to the preparation of adsorbents with high performances and low costs for economical and efficient wastewater treatment.

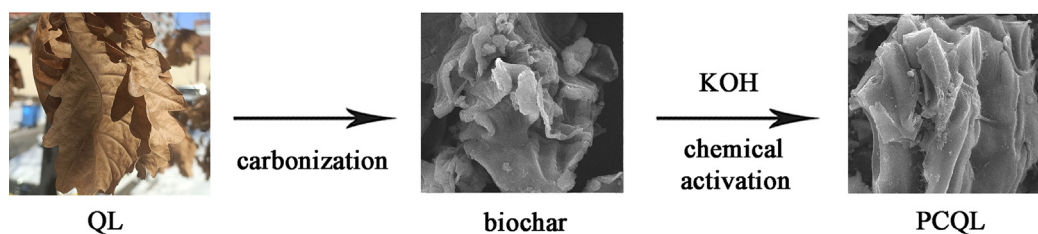
So far, biomass-derived adsorbents have attracted much attention because of the advantages of low cost, renewability, ready availability, and environmental friendliness (Benzigar et al., 2018). Various biomasses including leaves, grasses, woods, straws, and so on have been used as the precursors for preparing carbon materials toward the application of adsorption (Ahmad et al., 2020; Aichour et al., 2022; Dai et al., 2021). Through the processes of pyrolysis, these lignocellulosic biomasses can be converted to biochars which may effectively adsorb various pollutants from water (Dhyani and Bhaskar, 2018). However, the adsorption abilities of the biochars prepared via the simple carbonization processes were largely limited by their low specific surface areas and poor porosities. Thus, the biochars should be further activated utilizing various chemical activators (such as potassium hydroxide (KOH), sodium hydroxide (NaOH), zinc chloride (ZnCl<sub>2</sub>), etc.). A large number of pores may be formed in the surfaces of biochars through the reactions between carbon and chemical activators, which enable the produced porous carbon materials to exhibit extremely enhanced adsorption capacities toward pollutants (Chen et al., 2021; Wang et al., 2020). The activation processes inevitably increase the costs of adsorbents. However, the porous carbon products maintain the advantages of low costs and high performances. On one hand, the prices of some biomass precursors are close to zero. On the other

hand, after the activation processes, the specific surface areas and adsorption capacities of porous carbon materials may be several ten or hundred times higher than that of the biochars. This enables the biomass-derived porous carbons to be very competitive when they were utilized in certain relatively expensive devices such as household water filters, portable water filters, chromatographic columns, and so on.

Leaves may be readily obtained in many regions of the world. So far, various leaf-based adsorbents have been developed. Firstly, raw leaves may be directly used for adsorbing pollutants after the leaves had been washed, dried, and ground. For example, water bamboo leaves were used for removing methylene blue (MB) from water, and the maximum adsorption capacity was 54 mg g<sup>-1</sup> (Zhu et al., 2016). Bilberry (*Vaccinium myrtillus* L.) leaves were used for removing MB, and the maximum adsorption capacity was 200 mg g<sup>-1</sup> (Mosoarca et al., 2022). Secondly, leaves may be modified for improving their adsorption performances. For example, after being treated by NaOH and a surfactant, the fallen leaves of almond (*Prunus Dulcis*) were used for adsorbing Acid Blue 113, and the maximum adsorption capacity was 97 mg g<sup>-1</sup> (Jain and Gogate, 2017). Moreover, the leaves of several monocotyledons and dicotyledons were treated with ethanol and then used as the adsorbents. The maximum adsorption capacities of Cr (VI), Congo red, and RhB on the product derived from the leaves of *Forsythia suspensa* were 80, 233, and 75 mg g<sup>-1</sup>, respectively (Geng et al., 2022). Finally, leaves may be converted to carbon-based adsorbents. For example, the citric acid treated carbonized bamboo leaves powder was used for adsorbing MB, and the maximum adsorption capacity was 725 mg g<sup>-1</sup> (Ghosh and Bandyopadhyay, 2017). Furthermore, phosphoric acid (H<sub>3</sub>PO<sub>4</sub>) was used as the activator for preparing the activated carbon derived from *Gmelina aborea* leaves (GALAC). The maximum adsorption capacity of GALAC to RhB was 1000 mg g<sup>-1</sup>. (Bello et al., 2019). More work on the leaf-based adsorbents has been reviewed by Bulgariu and the co-authors (Bulgariu et al., 2019).

The leaf-derived porous carbon materials have exhibited high adsorption performances. However, the adsorption behaviours (such as adsorption capacities, kinetic models, and isotherm models) of various leaf-derived porous carbons are very different (Bulgariu et al., 2019; Yu et al., 2016). This may be due to that different leaves have different natural structures and chemical components. Thus, it is highly necessary to screen the leaf precursors for producing porous carbons with large surface areas and high performances toward the adsorption applications.

*Quercus mongolica* Fisch. ex Ledeb., an oak species, has been widely planted in East Asia (Yan et al., 2010). Herein, the *Quercus mongolica* leaf (QL) was used as the precursor for preparing porous carbon through the processes of carbonization and subsequently chemical activation (Scheme 1) with KOH and NaOH used as the activators, respectively. The produced porous carbon derived from the *Quercus mongolica* leaf (PCQL) was characterized through scanning electron microscopy (SEM), N<sub>2</sub> adsorption/desorption experiment, Fourier transform infrared (IR) spectroscopy, Raman spectroscopy, and X-ray photoelectron spectroscopy (XPS). Then, a representative dye (RhB) and a representative antibiotic (TC) were used as the model pollutants for evaluating the adsorption performances of PCQL



**Scheme 1** The preparation process of PCQL.

toward dyes and antibiotics. After the batch adsorption experiments were performed, the data were fitted by the three kinetic models (the pseudo-first-order, pseudo-second-order, and intra-particle diffusion models) and the four adsorption isotherm models (the Langmuir, Freundlich, Sips, and Redlich-Peterson (R-P) models). Moreover, the adsorption thermodynamics of adsorption processes, the reusability of PCQL, and the adsorption mechanism were studied. Finally, the feasibility of RhB adsorption on PCQL was investigated using the fixed-bed column study, and the Yoon-Nelson model was used to fit the experimental data.

## 2. Materials and methods

### 2.1. Materials

QLs were picked from *Quercus mongolica* planted in the campus of Jilin Agricultural University, China. All the reagents used in the experiments were analytical pure grade. They were directly used without additional purification.

### 2.2. Preparation of porous carbon

QLs were washed with water for removing dusts and other impurities adhered onto their surfaces. Then, they were dried at 80 °C in an oven. The dried QLs were smashed and filtered using a standard sieve (80 mesh). In the carbonization process, the QL powder was heated in a tube furnace at 500 °C for 60 min under N<sub>2</sub> flow. KOH and NaOH were used as the activators respectively. The biochar derived from QL was mixed with solid KOH (or NaOH) and then ground in a mortar. Then, the mixture was placed into a tube furnace and heated under N<sub>2</sub> flow. The adsorption performances of porous carbon products can be significantly influenced by the activation temperature, activation time, and the mass ratio of activator to carbon. In order to investigate the optimal activation conditions, the activation temperature was changed in the range of 700–900 °C, the mass ratio of KOH (or NaOH) to carbon was changed in the range of 3:1–5:1, and the activation time was changed in the range of 30–90 min. After the tube furnace was cooled, the sample was taken out and washed with HCl aqueous solution (1 M) and water repeatedly until the pH of filtrate was 7. Finally, the porous carbon product was dried and stored in a desiccator.

### 2.3. Characterization

The surface morphologies of samples were characterized using the scanning electron microscopy (Merlin, Zeiss, Germany). A Quantachrome Autosorb-iQ gas sorption analyzer (Quantachrome, USA) was used to perform the N<sub>2</sub> adsorption/des-

orption analyses, and the Brunauer-Emmer-Teller (BET) specific surface area and pore size distribution were measured. The porous carbon sample was characterized through Raman measurement using a LabRAM HR Evolution instrument (Horiba, France). The chemical bonds in the sample were confirmed based on the IR patterns which were obtained through utilizing a Nicolet iS5 FT-IR spectrophotometer (Thermo Fisher Scientific, USA). The surface chemical components of sample were characterized by XPS which was measured using an Axis Ultra DLD spectrometer (Kratos Analytical, UK).

### 2.4. Batch adsorption experiments

The samples of PCQL (20 mg) were added into the conical flasks with dye (or antibiotic) aqueous solutions (200 mL) with the initial concentrations of 100, 200, 300, and 400 mg g<sup>-1</sup>, respectively. The turbid liquids were shaken (160 rpm) in an air bath shaker under 30 °C. At pre-determined time, the samples (1 mL) were collected and centrifuged at 12000 rpm. The concentrations of supernatants were confirmed through measuring the adsorbances at 554 nm for RhB (or 357 nm for TC) using the UV-Vis spectrophotometer.

The equilibrium adsorption capacity of PCQL toward RhB (or TC),  $q_e$  (mg g<sup>-1</sup>), was calculated use Eq. (1).

$$q_e = \frac{(C_0 - C_e) \times V}{m} \quad (1)$$

where  $C_0$  (mg L<sup>-1</sup>) and  $C_e$  (mg L<sup>-1</sup>) are the initial and equilibrium concentrations of RhB (or TC) solution, respectively;  $V$  (L) and  $m$  (g) are the volume of RhB (or TC) solution and the mass of PCQL, respectively.

#### 2.4.1. Adsorption kinetic experiments

The effect of contact time on the adsorption capacities of PCQL toward RhB (or TC) was investigated through the pseudo-first-order, pseudo-second-order, and intra-particle diffusion models (Eqs. (2)–(4)) (Benjelloun et al., 2021).

$$q_t = q_e(1 - e^{-k_1 t}) \quad (2)$$

$$q_t = \frac{k_2 q_e^2 t}{1 + k_2 q_e t} \quad (3)$$

$$q_t = k_i t^{0.5} + C \quad (4)$$

where  $q_t$  (mg g<sup>-1</sup>) is the RhB (or TC) adsorption capacity of PCQL at contact time  $t$  (min);  $k_1$  (min<sup>-1</sup>) is the rate constant of the pseudo-first-order model;  $k_2$  (g mg<sup>-1</sup> min<sup>-1</sup>) is the rate constant of the pseudo-second-order model;  $k_i$  (mg g<sup>-1</sup> min<sup>-1/2</sup>) represents the rate constant of the intra-particle diffu-

sion kinetic model;  $C$  is the intercept in the linear relationship between  $q_t$  and  $t^{0.5}$ .

#### 2.4.2. Adsorption isotherm experiments

With the aim of investigating the effect of initial concentration of RhB (or TC) on the adsorption capacities of PCQL, the Langmuir, Freundlich, Sips, and R-P isotherm models (Eqs. (5)–(8)) (Majd et al., 2022) were used to fit the experimental data.

$$q_e = \frac{q_m K_L C_e}{1 + K_L C_e} \quad (5)$$

$$q_e = K_F C_e^{1/n_F} \quad (6)$$

$$q_e = \frac{q_m K_s C_e^{n_s}}{1 + K_s C_e^{n_s}} \quad (7)$$

$$q_e = \frac{K_{RP} C_e}{1 + \alpha_{RP} C_e^\beta} \quad (8)$$

where  $q_m$  ( $\text{mg g}^{-1}$ ) is the maximum adsorption capacity of PCQL toward RhB (or TC);  $K_L$  ( $\text{L mg}^{-1}$ ) is the equilibrium constant of the Langmuir model;  $K_F$  ( $\text{mg g}^{-1}(\text{L mg}^{-1})^{1/n}$ ) and  $n_F$  are the equilibrium constant and parameter of the Freundlich model, respectively;  $K_s$  ( $(\text{mg L}^{-1})^{-n}$ ) and  $n_s$  are the equilibrium constant and parameter of the Sips model, respectively;  $K_{RP}$  ( $\text{L mg}^{-1}$ ),  $\beta$ , and  $\alpha_{RP}$  ( $(\text{L mg}^{-1})^{-1/\beta}$ ) are the equilibrium constant and parameters of the R-P model, respectively.

#### 2.5. Adsorption thermodynamic experiments

For investing the adsorption thermodynamics during the adsorption processes. The adsorption experiments of PCQL toward RhB and TC were carried out at 30, 40, and 50 °C, respectively. The initial concentrations of RhB and TC aqueous solutions were both 400  $\text{mg L}^{-1}$ .

The adsorption enthalpy change ( $\Delta H$ ,  $\text{kJ mol}^{-1}$ ), standard entropy change ( $\Delta S$ ,  $\text{J mol}^{-1} \text{K}^{-1}$ ), and Gibbs free energy change ( $\Delta G$ ,  $\text{kJ mol}^{-1}$ ) were confirmed based on Eqs. (9)–(11) (Elmi et al., 2020).

$$\Delta G = \Delta H - T\Delta S \quad (9)$$

$$\ln(K_d) = \frac{\Delta S}{R} - \frac{\Delta H}{RT} \quad (10)$$

$$K_d = q_e/C_e \quad (11)$$

where  $T$  (K) is temperature;  $K_d$  is the distribution coefficient;  $R$  ( $\text{J K}^{-1} \text{mol}^{-1}$ ) is the ideal gas constant which is equal to 8.314.

#### 2.6. Reusability studies

The reusability of an adsorbent is important for its practical applications. In the reusability experiment, the sample of PCQL (100 mg) was added into a conical flask containing the aqueous solution of RhB (or TC) (50  $\text{mg L}^{-1}$ , 100 mL). The conical flask was shaken on a rotary shaker at 160 rpm under room temperature for 30 min. Then, the adsorbent was recovered through being filtered with a filtration membrane (0.22  $\mu\text{m}$ ). The residual concentration of RhB (or TC)

in solution was determined by measuring the adsorbance at 554 nm for RhB (or 357 nm for TC) using the UV–Vis spectrophotometer. The removal efficiency of RhB (or TC) from aqueous solution was calculated as follows:

$$\text{Removal efficiency} = (C_0 - C_i)/C_0 \times 100\% \quad (12)$$

where  $C_0$  is the initial concentration of RhB (or TC) (50  $\text{mg L}^{-1}$ ), and  $C_i$  is the residual concentration of RhB (or TC) in solution.

The adsorbent was generated through heat treatment. After the adsorbent was used, it was dried at 80 °C and further heated in a tube furnace at 500 °C for 60 min under  $\text{N}_2$  flow. Through the heat treatment, the RhB (or TC) adsorbed on PCQL was carbonized. After the furnace was cooled to room temperature, the adsorbent was taken out and used in the next adsorption cycles.

#### 2.7. The point of zero charge (PZC) of PCQL

A series of NaCl aqueous solutions (0.01 M) with pH values of 3, 5, 7, 9, and 11, respectively, were prepared and placed in different flasks. HCl or NaOH had been added for adjusting the pH values. The PCQL samples (0.1 g) were added into these solutions (50 mL), respectively. The flasks were sealed and shaken in a shaker at 160 rpm under room temperature for 24 h. The  $\text{pH}_{\text{PZC}}$  is determined by the intersection of the  $\text{pH}_{\text{initial}}$  and  $\text{pH}_{\text{final}}$  curves (Taoufik et al., 2019).

#### 2.8. Fixed-bed adsorption column study

The PCQL samples (0.25, 0.50, and 1.00 g) were added into the glass tubes with an inner diameter of 1.2 cm. The RhB (or TC) aqueous solutions (200  $\text{mg L}^{-1}$ ) were transfused into the tubes from the upper ends with the downward flow rate of 3.20  $\text{mL min}^{-1}$ . The concentrations of effluent RhB (or TC) solutions were monitored at the wavelength of 554 nm for RhB (or 357 nm for TC) using the UV–Vis spectrophotometer.

When the RhB (or TC) concentration of effluent solution reached 10% (20  $\text{mg L}^{-1}$ ) of the initial concentration, the time was called the breakthrough time ( $t_b$ , min), and the adsorption capacity of PCQL was expressed as  $q_b$  ( $\text{mg g}^{-1}$ ). Correspondingly, when the RhB (or TC) concentration of effluent solution reached 90% (180  $\text{mg L}^{-1}$ ) of the initial concentration, the time was called the saturation time ( $t_s$ , min), and the adsorption capacity of PCQL was expressed as  $q_s$  ( $\text{mg g}^{-1}$ ).

$$q_b = \frac{Q}{1000} \frac{C_0}{m} \int_{t=0}^{t=t_b} \left(1 - \frac{C_t}{C_0}\right) dt \quad (13)$$

$$q_s = \frac{Q}{1000} \frac{C_0}{m} \int_{t=0}^{t=t_s} \left(1 - \frac{C_t}{C_0}\right) dt \quad (14)$$

where  $C_0$  ( $\text{mg L}^{-1}$ ) represents the initial RhB (or TC) concentration;  $C_t$  ( $\text{mg L}^{-1}$ ) represents the RhB (or TC) concentration of effluent solution at time  $t$  (min);  $Q$  ( $\text{mL min}^{-1}$ ) is the flow rate;  $m$  (g) is the mass of PCQL (Jaria et al., 2019).

The treated effluent volume  $V_t$  (L) was calculated based on  $Q$  and  $t_s$ , and the percentage of fractional bed utilization (FBU, %) was calculated using  $q_b$  and  $q_s$ .

$$V_t = Q t_s \quad (15)$$

$$FBU = \left( \frac{q_b}{q_s} \right) \times 100\% \quad (16)$$

The non-linear Yoon-Nelson model was used to fit the experimental data obtained in the fixed-bed experiments.

$$\frac{C_i}{C_0} = \frac{1}{1 + \exp(k_{YN}(\tau - t))} \quad (17)$$

where  $\tau$  (min) is the time when 50% of RhB breakthrough happened;  $k_{YN}$  ( $\text{min}^{-1}$ ) is the rate constant (Aichour et al., 2019).

### 2.9. Error analysis

For determining which kinetic and isotherm models fit the experimental data well, the correlation coefficient ( $R^2$ ) and the sum of the squares of the errors ( $SSE$ ) were calculated based on the following formulas:

$$R^2 = \frac{\sum_{i=1}^n (q_{exp,i} - q_{ave})^2 - \sum_{i=1}^n (q_{exp,i} - q_{cal,i})^2}{\sum_{i=1}^n (q_{exp,i} - q_{ave})^2} \quad (18)$$

$$SSE = \sum_{i=1}^n (q_{cal,i} - q_{exp,i})^2 \quad (19)$$

where  $q_{exp,i}$ ,  $q_{cal,i}$ , and  $q_{ave}$  are the experimental, theoretical, and average adsorption capacities ( $\text{mg g}^{-1}$ ) of PCQL toward RhB (or TC), respectively.

## 3. Results and discussion

### 3.1. Preparation of porous carbon

After QL was carbonized under  $\text{N}_2$ , the produced biochar may effectively adsorb RhB and TC from water. However, the adsorption capacities of the biochar toward these pollutants were lower than  $50 \text{ mg g}^{-1}$ , when the initial concentrations of RhB and TC were  $400 \text{ mg L}^{-1}$ . In order to obtain the adsorbent with higher adsorption performances, the biochar was further chemically activated. The effect of the species of activator, activation temperature, the activator to carbon ratio, and activation time on the adsorption capacities of adsorbent samples were studied.

Initially, the biochar was activated using KOH as the activator. After solid KOH and the biochar were mixed and ground, the mixture was heated under  $\text{N}_2$ . Under suitable temperature and anaerobic conditions, a series of chemical reactions can take place (Eqs. (20)–(24)), which can result in the presence of abundant pores in the surface of carbon (Wang and Kaskel, 2012).



As shown in Fig. 1a, when the activation temperature increased from 700 to 800 °C, the RhB adsorption capacity of product increased from 981.2 to 1294.5  $\text{mg g}^{-1}$ . However,

when the temperature increased to 900 °C, the RhB adsorption capacity decreased to 984.5  $\text{mg g}^{-1}$ . This indicates that the adsorption performances of porous carbon products were largely affected by the activation temperature. The increment of temperature could increase the chemical reaction rates. As reported by Li et al.,  $\text{N}_2$  adsorption experiments indicated that suitable increment of activation temperature could increase the surface area and pore volume of product. However, excessively high activation temperature may decrease the surface area and pore volume, which might be due to the contraction or collapse of pores (Li et al., 2014). With the increase of porosity, the porous carbon product exhibited enhanced RhB adsorption capacity. Conversely, with the decrease of porosity, the porous carbon product exhibited reduced RhB adsorption capacity (Chen et al., 2018). As a result, the optimal activation temperature was confirmed to be 800 °C.

As shown in Fig. 1b and 1c, the adsorption capacities of carbon products were also affected by the dosage of KOH and the activation time. Suitable increment of the KOH to carbon ratio and the activation time may increase the RhB adsorption capacities of products, and extremely high KOH dosage and extremely long activation time may decrease the adsorption capacities. It was found that the optimal ratio of KOH to carbon and the optimal reaction time should be 4: 1 and 60 min, respectively.

Then, KOH was replaced with NaOH, and the effects of activation conditions on the RhB adsorption capacities of porous carbon products were shown in Fig S1 in the supporting information (SI). Through being heated under anaerobic condition, the biochar may react with NaOH forming the pores in the surface of biochar. The possible chemical equations were listed in Eqs. S1-S3 in SI. As a result, when NaOH was used as the activator, the optimal activation temperature was 800 °C, the optimal mass ratio of NaOH to biochar was 4:1, and the optimal heating time was 60 min. The RhB adsorption capacity of the product activated under the above conditions reached 943.5  $\text{mg g}^{-1}$ .

Moreover, potassium acetate and sodium acetate were also used as the activators. However, the corresponding RhB adsorption capacities of products were always lower than  $600 \text{ mg g}^{-1}$ , when the activation temperature was in the range of 700–900 °C. Thus, KOH was confirmed to be the best one among these chemical activators, because the porous carbon product activated by KOH exhibited the highest RhB adsorption capacity among the products activated by these activators. In the following adsorption experiments, the PCQL samples were prepared through using KOH as the activator.

### 3.2. Characterization

As shown in Fig. 2a and 2b, the powder of QL exhibited the corrugation geometries. After the chemical activation, the surfaces of sample had been obviously etched by KOH (Fig. 2c). Moreover, it seems that abundant tiny pores were formed (Fig. 2d). The porosity of PCQL was further investigated through  $\text{N}_2$  adsorption experiment (Fig. 3). The BET specific surface area of PCQL achieved  $3275 \text{ m}^2 \text{ g}^{-1}$ , the pore volume calculated based on the density functional theory (DFT) method reached  $1.8 \text{ cm}^3 \text{ g}^{-1}$ , and the average pore diameter was 2.5 nm. As shown in the pore size distribution curve

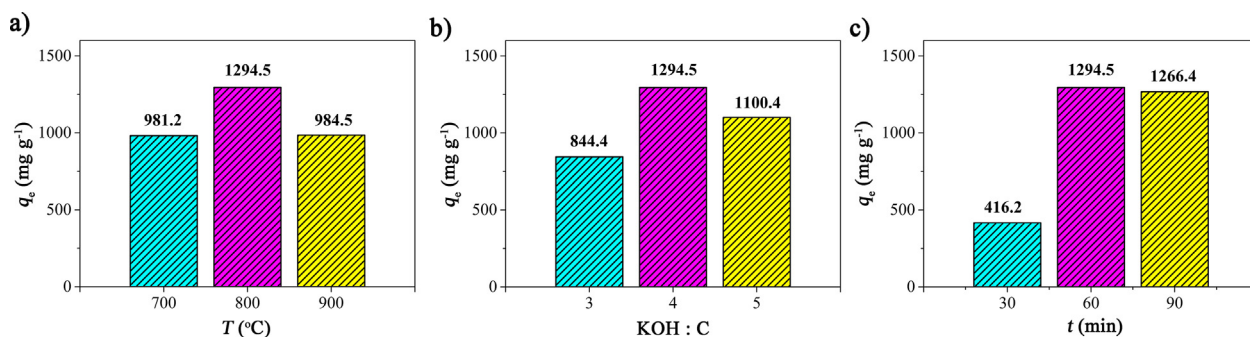


**Fig. 1** The relationship between the RhB adsorption capacities of porous carbon products and the activation conditions including (a) activation temperature, (b) the ratio of KOH to carbon, and (c) activation time with KOH used as the activator.

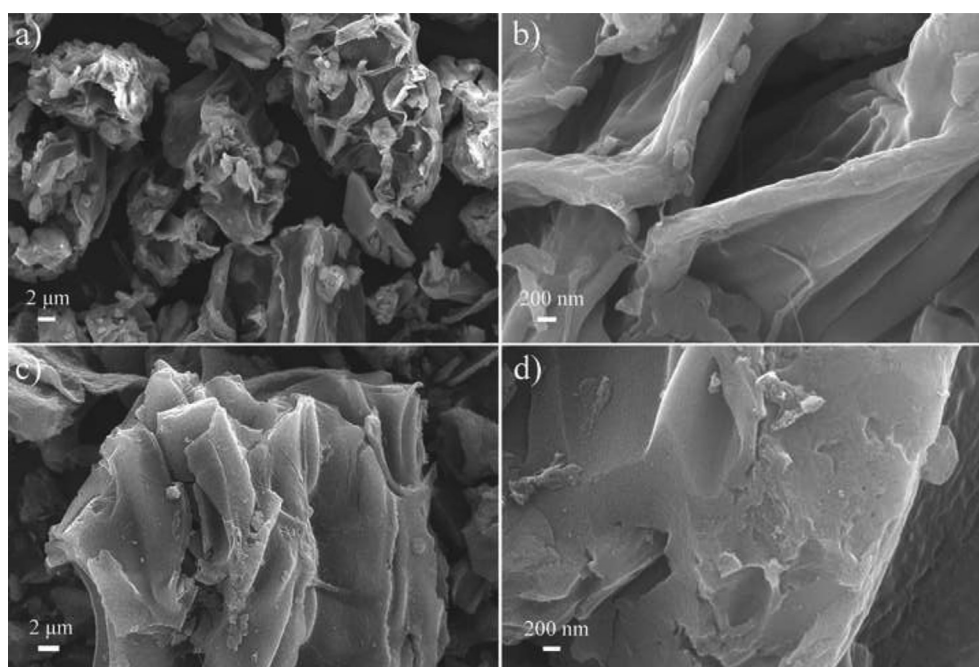


**Fig. 2** SEM images of (a and b) QL and (c and d) PCQL.

(Fig. 3b), both micropores and mesopores were formed in the surface of product after the chemical activation process.

In the Raman pattern of PCQL (Fig. 4a), the characteristic peaks at  $\sim 1360 \text{ cm}^{-1}$  (D-band) and  $\sim 1580 \text{ cm}^{-1}$  (G-band) may be assigned to the disordered carbon and crystalline carbon, respectively. The intensity ratio of  $I_D/I_G$  was close to 1.0. This means that PCQL was consisted of carbon with both defective graphitic structures and graphitic layers (Su et al., 2020).

The samples of QL and PCQL were also characterized by IR (Fig. 4b). The peaks at  $3425$ ,  $2920$ ,  $1739$ ,  $1620$ , and  $1022 \text{ cm}^{-1}$  in the IR pattern of QL may be attributed to the  $-\text{OH}$ ,  $\text{C}-\text{H}$ ,  $\text{C}=\text{O}$ ,  $\text{C}=\text{C}$ , and  $\text{C}-\text{O}$  stretching vibration, respectively. This is similar with the IR patterns of other biomasses which are mainly composed of lignin, hemicellulose, and cellulose (Tran et al., 2020; Vu et al., 2018). PCQL was derived from QL, and thus it exhibited similar IR pattern compared with that of QL. However, when the IR patterns were

measured, the sample of PCQL exhibited obviously weaker peak intensities comparing with that of the sample of QL, though the same mass of samples were used. This indicates that partial chemical bands on the surface of carbon have been destroyed during the activation process.

Moreover, the types of elements and functional groups in the surface of PCQL were investigated using XPS spectrum (Fig. S2 in SI). The elements of C and O were detected. Furthermore, the high-resolution C 1s spectrum may be fitted into five individual peaks at  $289.4$ ,  $286.5$ ,  $285.4$ ,  $284.9$  and  $284.4 \text{ eV}$ , respectively, which may be attributed to the  $\text{O}-\text{C}=\text{O}$ ,  $\text{C}=\text{O}$ ,  $\text{C}-\text{O}$ ,  $\text{C}=\text{C}$ , and  $\text{C}-\text{C}$  groups, respectively; the high-resolution O 1s spectrum may be fitted into three individual peaks at  $534.2$ ,  $533.3$ , and  $532.3 \text{ eV}$ , respectively, which may be attributed to the  $-\text{OH}$ ,  $-\text{C}-\text{O}$ , and  $-\text{C}=\text{O}$  groups, respectively (Ling et al., 2017; Ma et al., 2020). The conclusion drawn through the XPS characterization is consistent with the results of IR characterization.

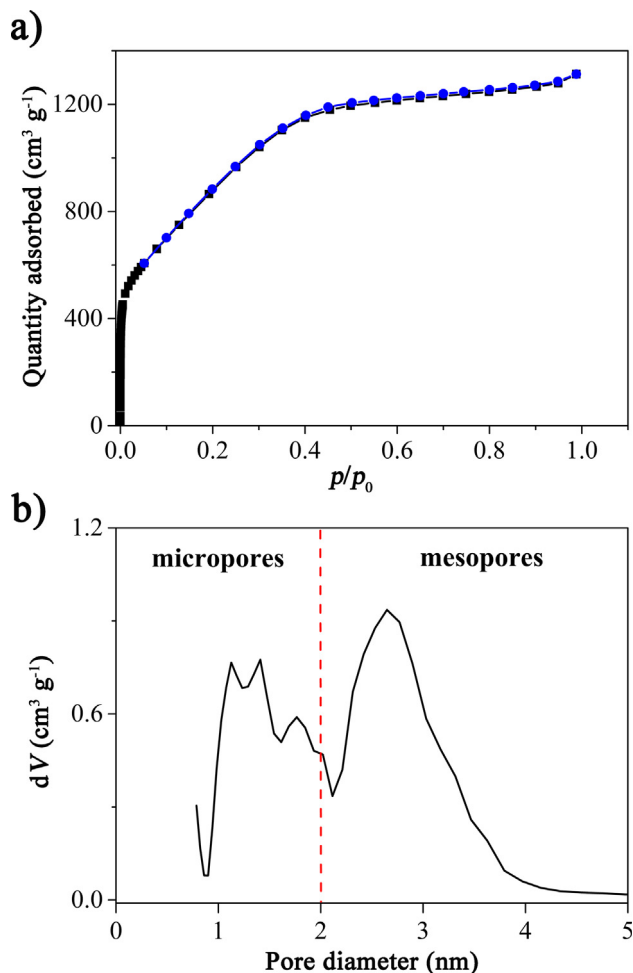


**Fig. 3** (a)  $N_2$  adsorption/desorption isotherms and (b) the pore size distribution curve of PCQL.

### 3.3. Batch adsorption experiments

#### 3.3.1. Adsorption kinetic models

As shown in Fig. 5, RhB and TC may be rapidly and effectively adsorbed by PCQL. In the first 20 min, the RhB adsorption capacities of PCQL reached 787.1, 989.5, 1078.4, and 1179.4  $\text{mg g}^{-1}$ , respectively, when the initial concentrations of RhB were 100, 200, 300, and 400  $\text{mg L}^{-1}$ , respectively (Fig. 5a). Then, the RhB adsorption capacities increased gradually and reached 890.1, 1153.4, 1245.8, and 1294.6  $\text{mg g}^{-1}$ , respectively, at the adsorption equilibrium. Along with the increase in RhB concentration, there was more opportunity for the surface of adsorbent to contact with RhB molecules, which resulted in higher adsorption capacities. When the adsorption of PCQL toward TC was studied, the similar trend was observed (Fig. 5b).

As shown in Fig. 5a and 5c, when two non-linear adsorption kinetic models were used to fit the adsorption capacities of PCQL toward RhB, the adsorption curve of the pseudo-second-order kinetic model matched the experimental data better than that of the pseudo-first-order kinetic model. When the pseudo-first-order kinetic model was used, the correlation coefficient ( $R^2$ ) values were in the range of 0.9895–0.9947,

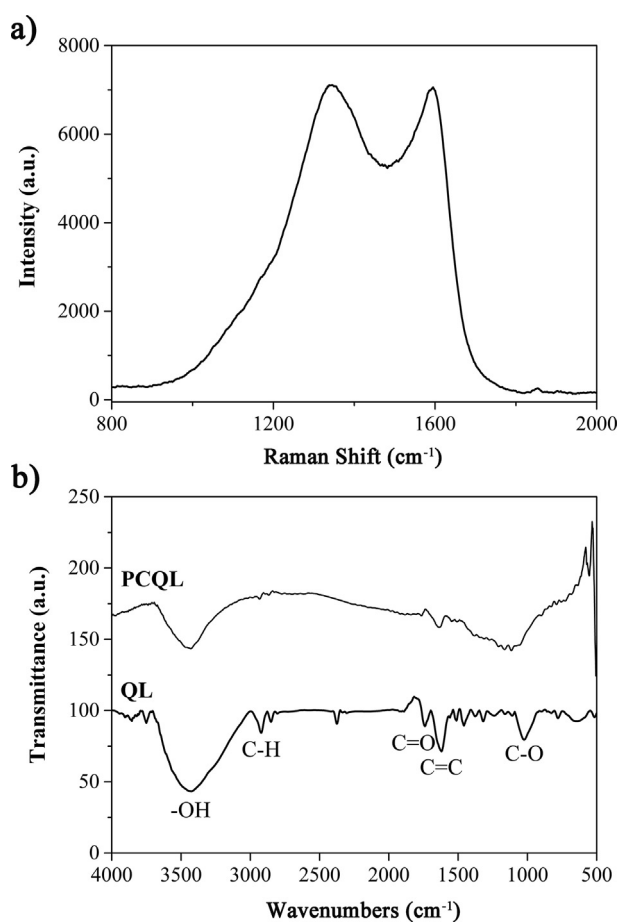


**Fig. 4** (a) Raman pattern of PCQL and (b) IR patterns of QL and PCQL.

and the  $SSE$  values were in the range of 508.48–1354.07. When the pseudo-second-order kinetic model was used, the  $R^2$  values were in the range of 0.9998–0.9999, and the  $SSE$  values were in the range of 5.26–12.61 (Table S1 in SI). Thus, the pseudo-second-order kinetic model fits the experimental data better than the pseudo-first-order kinetic model because of the higher  $R^2$  values and the lower  $SSE$  values. In addition, the equilibrium adsorption capacities (Table S1 in SI) calculated based on the pseudo-second-order kinetic model were close to the experimental equilibrium adsorption capacities. Thus, it is reasonable to use the pseudo-second-order model to fit the experimental data (Gülen et al., 2016).

For the adsorption of TC on PCQL, when the pseudo-second-order model was used for experimental data fitting, the calculated equilibrium adsorption capacities were close to the practical equilibrium adsorption capacities. Moreover, higher  $R^2$  values, lower  $SSE$  values, and better match between the calculated adsorption curve and the experimental data were achieved, comparing with the results obtained through using the pseudo-first-order model (Table S2 and Fig. 5b and 5d). Thus, the pseudo-second-order model was also better than the pseudo-first-order model for fitting the experimental data of PCQL adsorption toward TC.

The agreement between the experimental data and the pseudo-second-order kinetic model indicates that the adsorption processes of PCQL toward adsorbates were controlled

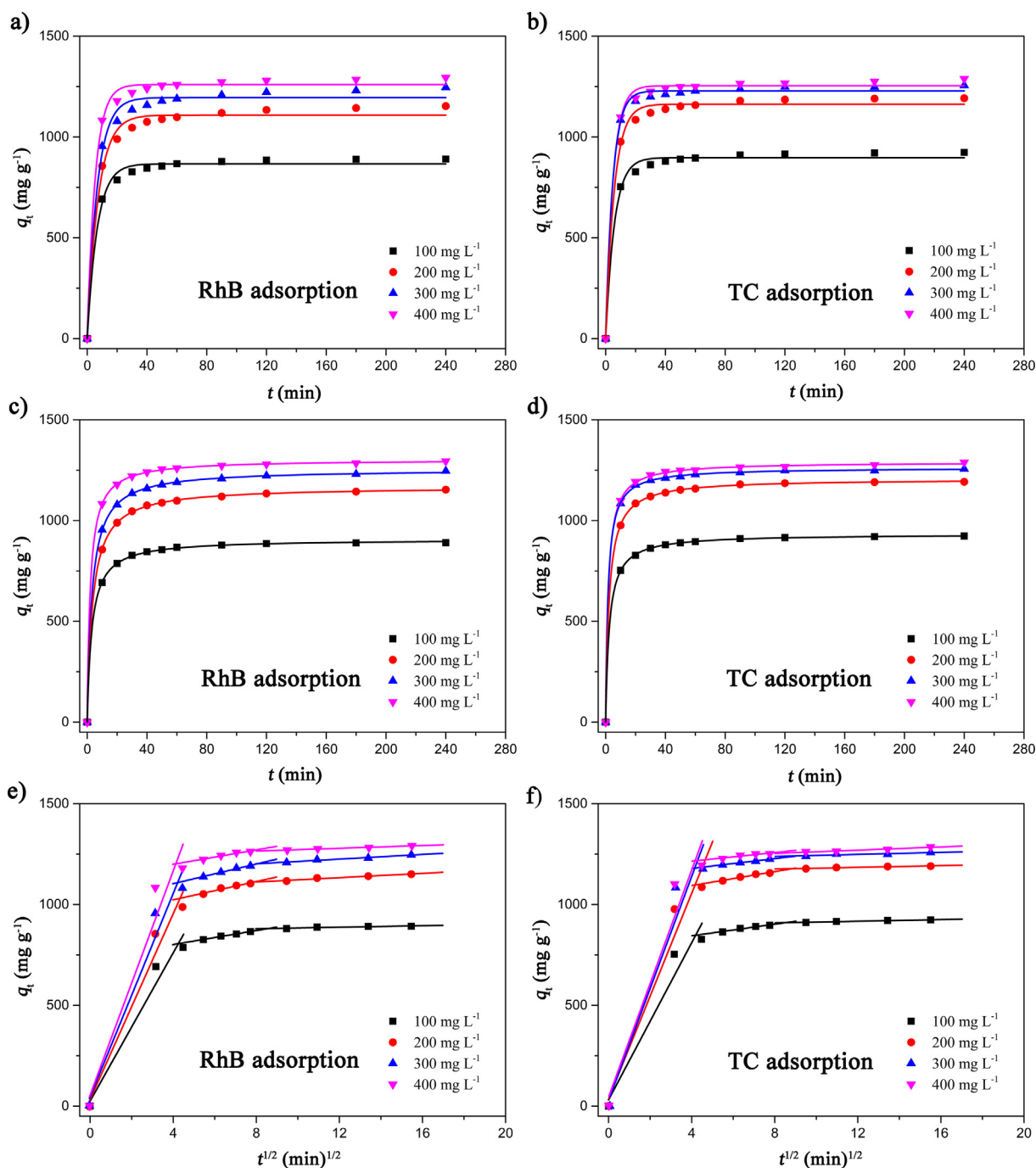


**Fig. 5** The relationship between the contact time and the adsorption capacities of PCQL toward (a, c, and e) RhB and (b, d, and f) TC. The experimental data were fitted by the (a and b) pseudo-first-order, (c and d) pseudo-second-order, and (e and f) intra-particle diffusion kinetic models, respectively.

by the amount of the adsorption active sites on the surface of PCQL (Zhao et al., 2020). Because of the large surface area, there are a large number of active sites exposed on the surface of PCQL, which may facilitate the removal of RhB and TC from water.

Moreover, the relationships between the contact time and the adsorption capacities were analyzed using the intra-particle diffusion model (Martins et al., 2015). As shown in the Fig. 5e and 5f, the regressions of  $q_t$  versus  $t^{1/2}$  may be

divided into three straight lines over the total adsorption processes, which indicates that the adsorption processes of PCQL toward the adsorbates may be segmented into different kinetics stages (Gülen et al., 2016). Firstly, the RhB (or TC) diffused to the external surface of PCQL. Secondly, the RhB (or TC) was gradually adsorbed by PCQL, and the adsorption rate was controlled by the intraparticle diffusion. Finally, the adsorption of RhB (or TC) on PCQL gradually reached adsorption equilibrium.

### 3.3.2. Adsorption isotherm models

Adsorption isotherm models may be applied for estimating the adsorption capacities of adsorbents and investigating the adsorption processes. Herein, several non-linear models were utilized to fit the experimental results. The fitted curves were depicted in Fig. 6. As shown in Table 1, when the Langmuir, Freundlich, Sips, and R-P models were used to fit the equilibrium adsorption capacities of RhB on PCQL, the  $R^2$  values were 0.9135, 0.9926, 0.9999, and 0.9996, respectively, and the SSE values were 2698.25, 228.94, 2.17, and 9.72, respectively. When these models were applied to fit the data on the TC adsorption, the  $R^2$  values were 0.9540, 0.9715, 0.9999, and 0.9994, respectively, and the SSE values were 1132.78, 702.11, 1.90, and 13.50, respectively. As a result, the Sips model fits the experimental data of RhB (and TC) adsorption on PCQL well because of the highest  $R^2$  value and the lowest SSE value. This result implies that adsorption active sites on the surface of PCQL were not identical, and these active sites have different affinities for the adsorbates (Haciosmanoğlu, et al., 2019). Moreover, the adsorption processes of PCQL toward RhB (or TC) may be divided into two stages based on the Sips model. In the RhB (or TC) solutions with lower concentrations, the multilayer adsorption occurred on the surfaces of PCQL; In the RhB (or TC) solutions with higher con-

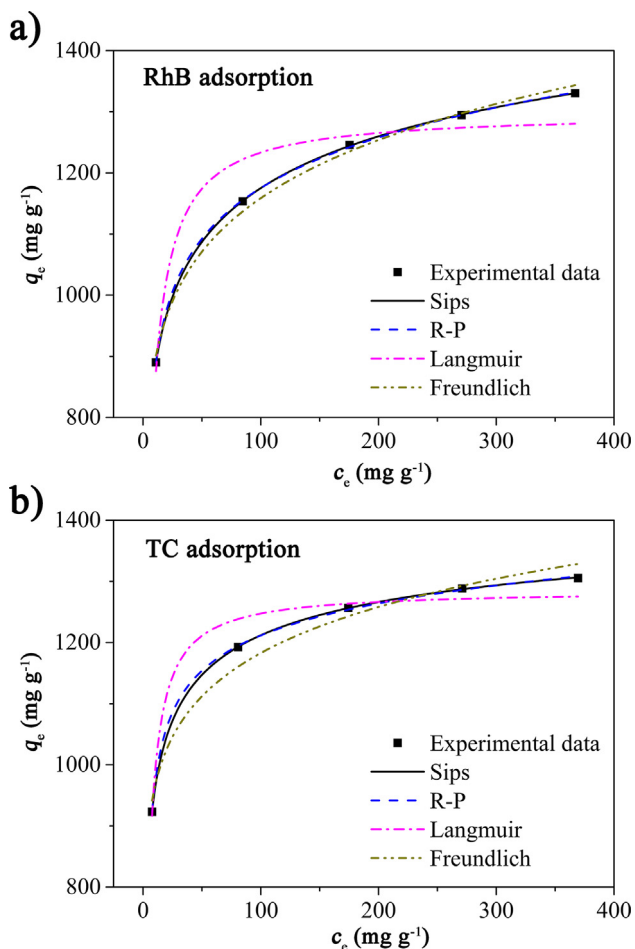


**Fig. 6** The relationships between the equilibrium concentrations of adsorbates and the equilibrium adsorption capacities of PCQL toward (a) RhB and (b) TC. The data were fitted by the Langmuir, Freundlich, Sips, and R-P isotherm models, respectively.

**Table 1** Parameters of isotherm models for RhB and TC adsorption on PCQL.

Isotherm models	Parameters	Adsorbates	
		RhB	TC
Langmuir	$Q_m$ (mg g <sup>-1</sup> )	1298.9	1286.0
	$K_L$ (L mg <sup>-1</sup> )	0.19	0.32
	$R^2$	0.9135	0.9540
	SSE	2698.25	1132.78
Freundlich	$K_F$ (mg g <sup>-1</sup> (L mg <sup>-1</sup> ) <sup>1/n</sup> )	686.30	785.28
	$n_F$	8.79	11.24
	$R^2$	0.9926	0.9715
	SSE	228.94	702.11
Sips	$q_m$ (mg g <sup>-1</sup> )	1946.0	1479.6
	$K_s$ (mg L <sup>-1</sup> ) <sup>-n</sup>	0.05	0.47
	$n_s$	0.27	0.39
	$R^2$	0.9999	0.9999
	SSE	2.17	1.90
R-P	$K_{RP}$ (L g <sup>-1</sup> )	898.35	828.43
	$b_{RP}$ (L mg <sup>-1</sup> ) <sup>-1/α</sup>	1.14	0.85
	$α$	0.91	0.95
	$R^2$	0.9996	0.9994
	SSE	9.72	13.50

centrations, the monolayer adsorption occurred on the surfaces of PCQL. According to the Sips model, the maximum adsorption capacities of PCQL towards RhB and TC were calculated to be 1946.0 and 1479.6 mg g<sup>-1</sup>, respectively.

As shown in Tables 2 and 3, the specific surface area and the maximum adsorption capacities of PCQL toward RhB and TC were compared with other adsorbents, respectively. Among these materials, PCQL exhibited the largest specific surface area. Its adsorption capacities were higher than most adsorbents and comparable with the graphene-based materials. This demonstrates that PCQL may be considered as a

**Table 2** Specific surface areas and maximum RhB adsorption capacities of different adsorbents.

Adsorbents	BET specific surface area (m <sup>2</sup> g <sup>-1</sup> )	Adsorption capacity (mg g <sup>-1</sup> )	Ref.
Magnetic <i>Forsythia suspensa</i> leaf powders	–	34	Geng and Chang, 2020
Activated carbon derived from white sugar	1148	123	Xiao et al., 2020
Graphite oxide	23	155	Jin et al., 2012
Rice husk-based activated carbon	1803	518	Ding et al., 2014
Lotus leaf porous carbon	2440	719	Li et al., 2020
Activated carbon prepared from <i>Gmelina aborea</i> leaves	–	1000	Bello et al., 2019
Porous carbon derived from corn straw	1993	1578	Chen et al., 2019
PCQL	3275	1946	This work

**Table 3** Specific surface areas and maximum TC adsorption capacities of different adsorbents.

Adsorbents	BET specific surface area ( $\text{m}^2 \text{g}^{-1}$ )	Adsorption capacity ( $\text{mg g}^{-1}$ )	Ref.
Biochar derived from rice husk	118	59	Liu et al., 2012
Multi-walled carbon nanotube	222	253	Babaei et al., 2016
Graphene oxide	–	323	Ghadim et al., 2013
Petroleum coke-derived porous carbon	2900	1122	Zhang et al., 2015
PCQL	3275	1480	This work
Magnetic graphene oxide/ZnO nanocomposite	–	1590	Qiao et al., 2020

promising adsorbent with the advantages of high performance and low cost.

### 3.4. Reusability

The utilization of the adsorbent with high reusability may economize the cost of wastewater treatment. Therefore, the reusability of PCQL for the adsorption of RhB and TC was investigated. Usually, after an adsorbent had been used for adsorbing pollutants, it was regenerated through being washed with water and/or organic solvents repeatedly for removing adsorbates from the surface of adsorbent. However, the eluates containing pollutants should be treated in an appropriate manner. Otherwise, there is the risk of secondary contamination.

In this work, based on the above consideration, after the sample of PCQL had been used for adsorbing RhB or TC, the recovered sample was dried and further heated at  $500^\circ\text{C}$  under  $\text{N}_2$  flow. Through the heat treatment, the RhB and TC molecules adsorbed by PCQL were carbonized for eliminating their potential hazards to the environment. Then, the sample was used as the adsorbent in the next adsorption cycle. As shown in Fig. 7, after five adsorption cycles, the removal efficiencies of PCQL toward RhB and TC decreased from 99% to about 90%. This result indicates that PCQL had good reusability.

### 3.5. Adsorption thermodynamics

The effect of environmental temperature on the adsorption capacities of PCQL toward RhB and TC was investigated. When the temperature increased from  $30$  to  $50^\circ\text{C}$ , the RhB adsorption capacity of PCQL increased from  $1278.5$  to  $1359.0 \text{ mg g}^{-1}$ . According to the linear relationship between  $\ln(q_e/C_e)$  and  $1/T$  (Eqs. (9)–(11)), the values of  $\Delta H$  and  $\Delta S$  were confirmed, and the results were shown in Table 4.

In the process of RhB adsorption on PCQL, the value of  $\Delta H$  was  $2.12 \text{ kJ mol}^{-1}$ . On one hand, the attachment of RhB ions on the surface of PCQL should be exothermic. On the other hand, the RhB ions are surrounded by the solvation sheaths. When RhB ions were attached by PCQL, some water

molecules in the solvation sheath had to leave. Thus, the positive value of  $\Delta H$  might mean that the energy consumed in the dehydration process was higher than the energy released in the process of attaching RhB ions to the surface of PCQL (Anastopoulos and Kyzas, 2016). The magnitude of  $\Delta H$  may be used for evaluating the type of adsorption processes. The value of  $\Delta H$  is much lower than  $40 \text{ kJ mol}^{-1}$ . The relatively low adsorption heat indicates the process of RhB adsorption on PCQL may be categorized as physisorption (Elmi et al., 2020; Salaa et al., 2020).

The value of  $\Delta S$  was  $20.02 \text{ J mol}^{-1} \text{ K}^{-1}$ . The positive value of  $\Delta S$  suggested increased randomness in the solid/solution interface during the process of RhB adsorption on PCQL. One possible reason is that one water molecule on the surface of PCQL was replaced by more water molecules, resulting in the increase in entropy (Anastopoulos and Kyzas, 2016; Nekouei et al., 2015; Shu et al., 2015).

When the environmental temperature increased gradually, the values of  $\Delta G$  decreased from  $-3.94$  to  $-4.34 \text{ kJ mol}^{-1}$ , which indicates that the adsorption processes are spontaneous and may be affected by temperature in some degree (Barkakati et al., 2010).

Similar to the RhB adsorption on PCQL, the adsorption of TC on PCQL was still a spontaneous physical process accom-

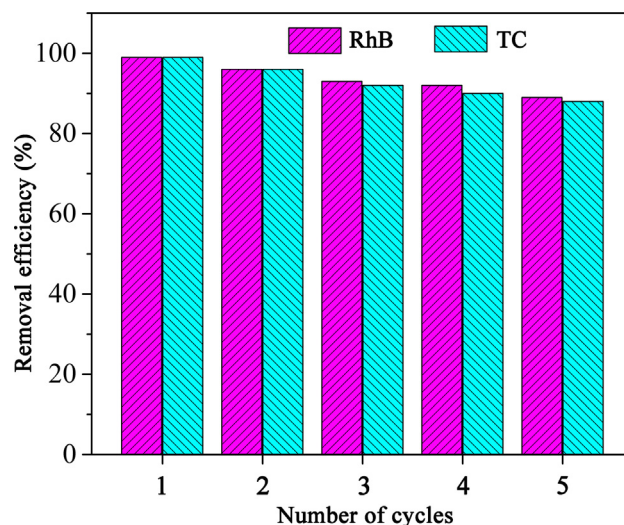


**Fig. 7** Reusability of PCQL for adsorbing RhB and TC ( $C_0 = 50 \text{ mg L}^{-1}$ ,  $V = 100 \text{ mL}$ , adsorbent mass =  $100 \text{ mg}$ ).

**Table 4** Thermodynamic parameters of PCQL adsorption toward RhB and TC.

Adsorbates	Temperature ( $^\circ\text{C}$ )	$\Delta H$ ( $\text{kJ mol}^{-1}$ )	$\Delta S$ ( $\text{J mol}^{-1}$ )	$\Delta G$ ( $\text{kJ mol}^{-1}$ )
RhB	30	2.12	20.02	-3.94
	40			-4.14
	50			-4.34
TC	30	-3.24	2.15	-3.89
	40			-3.92
	50			-3.94

panied by the increasing disorder degree. However, there are some differences. The TC adsorption capacities of PCQL slightly decreased along with the temperature increment, and the adsorption process was exothermal.

### 3.6. Adsorption mechanism

PCQL may effectively adsorb RhB and TC from water phase, which may be due to several possible reasons. At first, the result of  $N_2$  adsorption/desorption experiment indicates that PCQL had abundant micro- and mesopores, and the average pore diameter was 2.5 nm. Thus, the RhB and CAP molecules may diffuse into these pores and be captured by the adsorption active sites inside the pores. Secondly, the result of Raman spectrum proved the exist of abundant graphene layers in PCQL, and the value of  $I_G/I_D$  was close to 1.0. Therefore, the aromatic adsorbates may be attached on the graphene layers of PCQL through the  $\pi$ - $\pi$  interactions. Thirdly, as shown in the IR and XPS patterns, there are the —OH, C—O, and C=O groups on the surface of PCQL, and these groups may form strong interactions with RhB and TC through the hydrogen bonds. Finally, in order to investigate the charges on the surface of PCQL, the point of zero charge (PZC) was confirmed, and the  $pH_{PZC}$  is about 6.4 (Fig. S3a in SI). This result means that the surface charges of PCQL were positive when the pH of solution was lower than 6.4, and the surface charges of PCQL were negative when the pH of solution was bigger than 6.4. When PCQL was used to adsorb RhB in the aqueous solutions with pH in the range of 3–11, the adsorption capacities were only slightly changed (Fig. S2b in SI). This result means that the influence of electrostatic interaction may be ignored in the process of PCQL adsorption toward the adsorbate. In sum, the adsorption mechanism may be attributed to the combination of the pore-filling,  $\pi$ - $\pi$ , and hydrogen bond interactions.

### 3.7. Fixed-bed adsorption column study

In addition to the batch adsorption experiments, a series of fixed-bed column experiments were performed for removing RhB and TC from water using PCQL as the adsorbent. The concentrations of RhB and TC solutions were both  $200 \text{ mg L}^{-1}$ . The dosages of PCQL samples were 0.25, 0.50, and 1.00 g, respectively. When the dosage of PCQL was 1.00 g, the value (6.5) of height to diameter ratio ( $H/D$ ) was higher than 5. Under such condition, the maldistribution of the RhB solution in the adsorption process might be avoided (Penafiel et al., 2021). The non-linear Yoon-Nelson model was used to fit the experimental breakthrough curves, the  $R^2$  values were higher than 0.99, which demonstrates that this model fitted the experimental data well.

The experimental and simulated breakthrough curves of RhB adsorption on PCQL were shown in Fig. 8a. The breakthrough curves were obviously influenced by the dosages of adsorbent. Along with the increasement in adsorbent dosages, the breakthrough curves shifted to the right. As shown in Table 5, when the mass of adsorbent increased from 0.25 to 1.00 g, the breakthrough time increased from 460 to 2209 min, the value of  $\tau$  increased from 543 to 2338 min, the

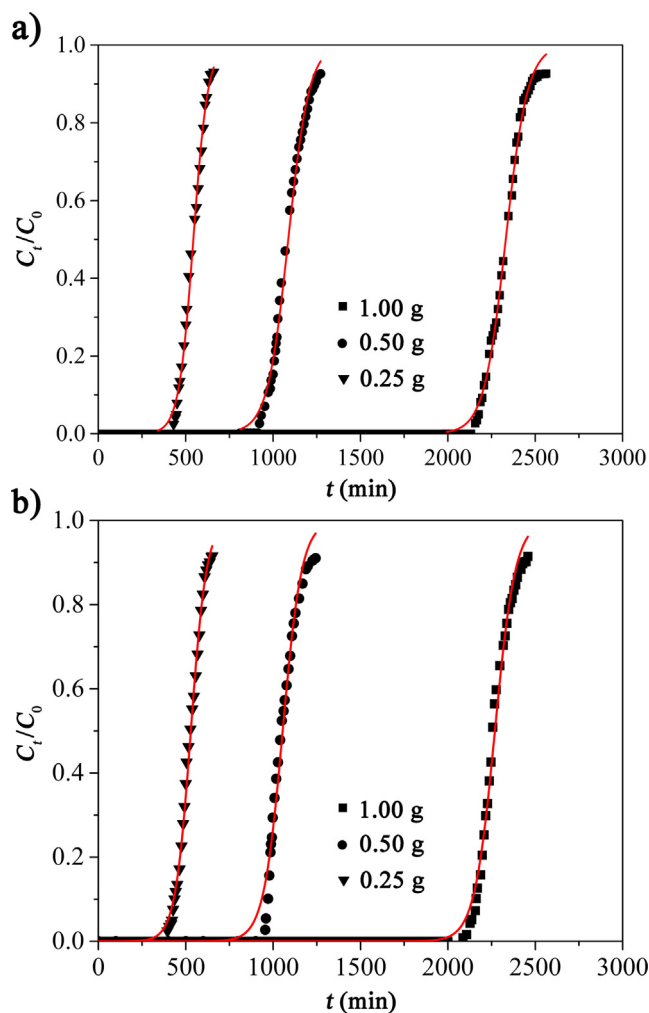


**Fig. 8** Breakthrough curves of adsorption of PCQL toward (a) RhB and (b) TC. The dosages of PCQL were 0.25 g, 0.5 g, and 1.0 g, respectively. The experimental data were fitted with the nonlinear Yoon-Nelson model.

exhaustion time increased from 630 to 2490 min, and the volume of treated wastewater increased from 2.02 to 7.97 L. A similar conclusion was drawn, when PCQS had been used for adsorbing TC in the column (Fig. 8b and Table 6). This may be attributed to the fact that the adsorbent with higher mass provided more adsorption active sites for the attachment of RhB and TC molecules. Thus, the column with more adsorbent may be used for longer time, and more volume of wastewater may be treated. Moreover, for both the RhB adsorption and the TC adsorption on PCQL, along with the increment of adsorbent dosage, the values of  $q_b$ ,  $q_s$ , and  $FBU$  increased. These results may be due to that, when the bed height increased, the axial dispersion of RhB and TC solutions decreased (Auta and Hameed, 2014; Chu, 2020). This would mean that greater mass (or greater bed height) of adsorbent brought more contact time, which enable the RhB and TC molecules to diffuse into the deeper pores of PCQL. That is to say, greater mass (or greater bed height) of adsorbent is benefit for better utilization of adsorbent.

**Table 5** Data of the fixed-bed experiments on removal of RhB from water (Diameter of column, 1.2 cm; flow rate, 3.2 mL min<sup>-1</sup>; initial concentration, 200 mg L<sup>-1</sup>).

<i>m</i> (g)	<i>H</i> (cm)	<i>H/D</i>	<i>c<sub>t</sub>/c<sub>0</sub></i> = 0.1		<i>c<sub>t</sub>/c<sub>0</sub></i> = 0.9		<i>FBU</i> (%)	<i>V<sub>t</sub></i> (L)	Yoon-Nelson model		
			<i>t<sub>b</sub></i> (min)	<i>q<sub>b</sub></i> (mg g <sup>-1</sup> )	<i>t<sub>s</sub></i> (min)	<i>q<sub>s</sub></i> (mg g <sup>-1</sup> )			<i>k</i> (min <sup>-1</sup> )	<i>τ</i> (min)	<i>R</i> <sup>2</sup>
0.25	2.0	1.7	460	1172.7	630	1384.1	84.7	2.02	0.024	543	0.9941
0.50	4.0	3.3	980	1250.1	1255	1401.9	89.2	4.02	0.017	1095	0.9933
1.00	7.8	6.5	2209	1414.6	2490	1495.2	94.6	7.97	0.016	2338	0.9965

**Table 6** Data of the fixed-bed experiments on removal of TC from water (Diameter of column, 1.2 cm; flow rate, 3.2 mL min<sup>-1</sup>; initial concentration, 200 mg L<sup>-1</sup>).

<i>m</i> (g)	<i>H</i> (cm)	<i>H/D</i>	<i>c<sub>t</sub>/c<sub>0</sub></i> = 0.1		<i>c<sub>t</sub>/c<sub>0</sub></i> = 0.9		<i>FBU</i> (%)	<i>V<sub>t</sub></i> (L)	Yoon-Nelson model		
			<i>t<sub>b</sub></i> (min)	<i>q<sub>b</sub></i> (mg g <sup>-1</sup> )	<i>t<sub>s</sub></i> (min)	<i>q<sub>s</sub></i> (mg g <sup>-1</sup> )			<i>k</i> (min <sup>-1</sup> )	<i>τ</i> (min)	<i>R</i> <sup>2</sup>
0.25	2.0	1.7	436	1109.6	638	1352.0	68.3	2.04	0.022	529	0.9960
0.50	4.0	3.3	971	1240.5	1225	1360.0	79.3	3.92	0.018	1055	0.9841
1.00	7.8	6.5	2162	1381.5	2438	1454.2	88.7	7.80	0.017	2269	0.9898

#### 4. Conclusion

It is the first time that QL was used as the precursor for preparing the hierarchical porous carbon material with large specific surface area and high adsorption ability toward the representative dye and antibiotic. KOH was better than NaOH as the chemical activator, and the BET specific surface area of PCQL activated by KOH reached 3275 m<sup>2</sup> g<sup>-1</sup>. The results of batch adsorption experiments indicate that the maximum adsorption capacities of PCQL toward RhB and TC were 1946.0 and 1479.6 mg g<sup>-1</sup>, respectively, based on the Sips model. The adsorption of PCQL toward adsorbates may be due to the combination of the pore-filling, hydrogen bond, and  $\pi$ - $\pi$  interactions. The results of fixed-bed experiments demonstrate that PCQL is highly effective for removing RhB and TC from water after it was filled in the column. About 8 L of wastewater containing RhB (or TC) with the initial concentration of 200 mg g<sup>-1</sup> may be treated using 1.0 g of PCQL. Thus, PCQL may be considered as a promising adsorbent with the advantages of high performance and low cost. In the future, we will further prepare various PCQL-contained composites for different applications. For example, PCQL will be combined with polymers for preparing the coating materials used for the controlled release of fertilizers and pesticides. PCQL will be used as the support for nanoscale zero-valent iron, and the produced composite material should be able to activate H<sub>2</sub>O<sub>2</sub> for achieving the catalytic degradation of organic pollutants. Additionally, the functional groups contain nitrogen (N), phosphorus (P), oxygen (O), boron (B), and sulphur (S) elements will be introduced to the surface of PCQL for optimizing the physical and chemical properties of porous carbon toward the application in supercapacitors.

#### Declaration of Competing Interest

The authors declare that they have no known competing financial interests or personal relationships that could have appeared to influence the work reported in this paper.

#### Acknowledgements

This work was supported by the Scientific Research Projects of the Education Department of Jilin Province (No. JJKH20220327KJ).

#### Appendix A. Supplementary material

Supplementary data to this article can be found online at <https://doi.org/10.1016/j.arabjc.2022.104031>.

#### References

- Abd El-Monaem, E.M., Eltaweil, A.S., Elshishini, H.M., Hosny, M., Abou Alsoaud, M.M., Attia, N.F., El-Subruiti, G.M., Omer, A.M., 2022. Sustainable adsorptive removal of antibiotic residues by chitosan composites: An insight into current developments and future recommendations. *Arab. J. Chem.* 15. <https://doi.org/10.1016/j.arabjc.2022.103743> 103743.
- Ahmad, A.A., Din, A.T.M., Yahaya, N.K.E., Khasri, A., Ahmad, M. A., 2020. Adsorption of basic green 4 onto gasified Glyricidia sepium woodchip based activated carbon: Optimization, characterization, batch and column study. *Arab. J. Chem.* 13, 6887–6903. <https://doi.org/10.1016/j.arabjc.2020.07.002>.
- Aichour, A., Zaghouane-Boudiaf, H., Djafer Khodja, H., 2022. Highly removal of anionic dye from aqueous medium using a promising biochar derived from date palm petioles: Characterization, adsorption properties and reuse studies. *Arab. J. Chem.* 15. <https://doi.org/10.1016/j.arabjc.2021.103542> 103542.
- Aichour, A., Zaghouane-Boudiaf, H., Zuki, F.B.M., Aroua, M.K., Viseras Ibbora, C., 2019. Low-cost, biodegradable and highly effective adsorbents for batch and column fixed bed adsorption processes of methylene blue. *J. Environ. Chem. Eng.* 7. <https://doi.org/10.1016/j.jece.2019.103409> 103409.
- Anastopoulos, I., Kyzas, G.Z., 2016. Are the thermodynamic parameters correctly estimated in liquid-phase adsorption phenomena? *J. Mol. Liq.* 218, 174–185. <https://doi.org/10.1016/j.molliq.2016.02.059>.
- Auta, M., Hameed, B.H., 2014. Chitosan–clay composite as highly effective and low-cost adsorbent for batch and fixed-bed adsorption of methylene blue. *Chem. Eng. J.* 237, 352–361. <https://doi.org/10.1016/j.cej.2013.09.066>.
- Babaei, A.A., Lima, E.C., Takdastan, A., Alavi, N., Goudarzi, G., Vosoughi, M., Hassani, G., Shirmardi, M., 2016. Removal of tetracycline antibiotic from contaminated water media by multi-walled carbon nanotubes: operational variables, kinetics, and

- equilibrium studies. *Water Sci. Technol.* 74, 1202–1216. <https://doi.org/10.2166/wst.2016.301>.
- Barkakati, P., Begum, A., Das, M.L., Rao, P.G., 2010. Adsorptive separation of ginsenoside from aqueous solution by polymeric resins: Equilibrium, kinetic and thermodynamic studies. *Chem. Eng. J.* 161, 34–45. <https://doi.org/10.1016/j.cej.2010.04.018>.
- Bello, O.S., Alabi, E.O., Adegoke, K.A., Adegboyega, S.A., Inyinbor, A.A., Dada, A.O., 2019. Rhodamine B dye sequestration using *Gmelina aborea* leaf powder. *Heliyon* 5, <https://doi.org/10.1016/j.heliyon.2019.e02872>.
- Benjelloun, M., Miyah, Y., Akdemir Evrendilek, G., Zerrouq, F., Lairini, S., 2021. Recent advances in adsorption kinetic models: Their application to dye types. *Arab. J. Chem.* 14, <https://doi.org/10.1016/j.arabjc.2021.103031>.
- Benzigar, M.R., Talapaneni, S.N., Joseph, S., Ramadass, K., Singh, G., Scaranto, J., Ravon, U., Al-Bahily, K., Vinu, A., 2018. Recent advances in functionalized micro and mesoporous carbon materials: synthesis and applications. *Chem. Soc. Rev.* 47, 2680–2721. <https://doi.org/10.1039/c7cs00787f>.
- Bulgariu, L., Escudero, L.B., Bello, O.S., Iqbal, M., Nisar, J., Adegoke, K.A., Alakhras, F., Kornaros, M., Anastopoulos, I., 2019. The utilization of leaf-based adsorbents for dyes removal: A review. *J. Mol. Liq.* 276, 728–747. <https://doi.org/10.1016/j.molliq.2018.12.001>.
- Chen, S.J., Tang, S.S., Sun, Y., Wang, G., Chen, H., Yu, X.X., Su, Y. J., Chen, G., 2018. Preparation of a highly porous carbon material based on quinoa husk and its application for removal of dyes by adsorption. *Materials* 11, 14. <https://doi.org/10.3390/ma11081407>.
- Chen, S., Chen, G., Chen, H., Sun, Y., Yu, X., Su, Y., Tan, S., 2019. Preparation of porous carbon-based material from corn straw via mixed alkali and its application for removal of dye. *Colloid. Surf. A* 568, 173–183. <https://doi.org/10.1016/j.colsurfa.2019.02.008>.
- Chen, S., Xia, Y., Zhang, B., Chen, H., Chen, G., Tang, S., 2021. Disassembly of lignocellulose into cellulose, hemicellulose, and lignin for preparation of porous carbon materials with enhanced performances. *J. Hazard. Mater.* 408, <https://doi.org/10.1016/j.jhazmat.2020.124956>.
- Chu, K.H., 2020. Breakthrough curve analysis by simplistic models of fixed bed adsorption: In defense of the century-old Bohart-Adams model. *Chem. Eng. J.* 380, <https://doi.org/10.1016/j.cej.2019.122513>.
- Dai, W., Xu, M., Zhao, Z., Zheng, J., Huang, F., Wang, H., Liu, C., Xiao, R., 2021. Characteristics and quantification of mechanisms of Cd<sup>2+</sup> adsorption by biochars derived from three different plant-based biomass. *Arab. J. Chem.* 14, <https://doi.org/10.1016/j.arabjc.2021.103119>.
- Dhyani, V., Bhaskar, T., 2018. A comprehensive review on the pyrolysis of lignocellulosic biomass. *Renew. Energ.* 129, 695–716. <https://doi.org/10.1016/j.renene.2017.04.035>.
- Ding, L., Zou, B., Gao, W., Liu, Q., Wang, Z., Guo, Y., Wang, X., Liu, Y., 2014. Adsorption of rhodamine-B from aqueous solution using treated rice husk-based activated carbon. *Colloid. Surf. A* 446, 1–7. <https://doi.org/10.1016/j.colsurfa.2014.01.030>.
- Dong, F., Pang, Z., Yang, S., Lin, Q., Song, S., Li, C., Ma, X., Nie, S., 2022. Improving wastewater treatment by triboelectric-photo/electric coupling effect. *ACS Nano* 16, 3449–3475. <https://doi.org/10.1021/acsnano.1c10755>.
- Elmi, F., Damghani, F.M., Taleshi, M.S., 2020. Kinetic and isotherm studies of adsorption of the metribuzin herbicide on an Fe<sub>3</sub>O<sub>4</sub>/CNT@PDA hybrid magnetic nanocomposite in wastewater. *Ind. Eng. Chem. Res.* 59, 9604–9610. <https://doi.org/10.1021/acs.iecr.9b07077>.
- Gadipelly, C., Pérez-González, A., Yadav, G.D., Ortiz, I., Ibáñez, R., Rathod, V.K., Marathe, K.V., 2014. Pharmaceutical industry wastewater: Review of the technologies for water treatment and reuse. *Ind. Eng. Chem. Res.* 53, 11571–11592. <https://doi.org/10.1021/ie501210j>.
- Gao, Y., Li, Y., Zhang, L., Huang, H., Hu, J., Shah, S.M., Su, X., 2012. Adsorption and removal of tetracycline antibiotics from aqueous solution by graphene oxide. *J. Colloid Interf. Sci.* 368, 540–546. <https://doi.org/10.1016/j.jcis.2011.11.015>.
- Geng, J., Chang, J., 2020. Synthesis of magnetic *Forsythia suspensa* leaf powders for removal of metal ions and dyes from wastewater. *J. Environ. Chem. Eng.* 8, <https://doi.org/10.1016/j.jece.2020.104224>.
- Geng, J., Lin, L., Gu, F., Chang, J., 2022. Adsorption of Cr(VI) and dyes by plant leaves: Effect of extraction by ethanol, relationship with element contents and adsorption mechanism. *Ind. Crop. Prod.* 177. <https://doi.org/10.1016/j.indcrop.2022.114522>.
- Ghadim, E.E., Manouchehri, F., Soleimani, G., Hosseini, H., Kimiagar, S., Nafisi, S., 2013. Adsorption properties of tetracycline onto graphene oxide: Equilibrium, kinetic and thermodynamic studies. *PLoS ONE* 8, <https://doi.org/10.1371/journal.pone.0079254>.
- Ghosh, S., Bandyopadhyay, A., 2017. Adsorption of methylene blue onto citric acid treated carbonized bamboo leaves powder: Equilibrium, kinetics, thermodynamics analyses. *J. Mol. Liq.* 248, 413–424. <https://doi.org/10.1016/j.molliq.2017.10.086>.
- Gülen, J., Akın, B., Özgür, M., 2016. Ultrasonic-assisted adsorption of methylene blue on sumac leaves. *Desalin. Water Treat.* 57, 9286–9295. <https://doi.org/10.1080/19443994.2015.1029002>.
- Haciosmanoğlu, G.G., Doğruel, T., Genç, S., Oner, E.T., Can, Z.S., 2019. Adsorptive removal of bisphenol A from aqueous solutions using phosphonated levan. *J. Hazard. Mater.* 374, 43–49. <https://doi.org/10.1016/j.jhazmat.2019.04.015>.
- Huang, Y., Zheng, X., Feng, S., Guo, Z., Liang, S., 2016. Enhancement of rhodamine B removal by modifying activated carbon developed from *Lythrum salicaria* L. with pyruvic acid. *Colloid. Surface. A* 489, 154–162. <https://doi.org/10.1016/j.colsurfa.2015.10.050>.
- Jain, S.N., Gogate, P.R., 2017. Acid Blue 113 removal from aqueous solution using novel biosorbent based on NaOH treated and surfactant modified fallen leaves of *Prunus Dulcis*. *J. Environ. Chem. Eng.* 5, 3384–3394. <https://doi.org/10.1016/j.jece.2017.06.047>.
- Jaria, G., Calisto, V., Silva, C.P., Victoria Gil, M., Otero, M., Esteves, V.I., 2019. Fixed-bed performance of a waste-derived granular activated carbon for the removal of micropollutants from municipal wastewater. *Sci. Total Environ.* 683, 699–708. <https://doi.org/10.1016/j.scitotenv.2019.05.198>.
- Jin, Q.Q., Zhu, X.H., Xing, X.Y., Ren, T.Z., 2012. Adsorptive removal of cationic dyes from aqueous solutions using graphite oxide. *Adsorpt. Sci. Technol.* 30, 437–447. <https://doi.org/10.1260/0263-6174.30.5.437>.
- Li, X.F., Xu, Q., Fu, Y., Guo, Q.-X., 2014. Preparation and characterization of activated carbon from kraft lignin via KOH activation. *Environ. Prog. Sustain.* 33, 519–526. <https://doi.org/10.1002/ep.11794>.
- Li, A., Huang, W., Qiu, N., Mou, F., Wang, F., 2020. Porous carbon prepared from lotus leaves as potential adsorbent for efficient removal of rhodamine B. *Mater. Res. Express* 7, <https://doi.org/10.1088/2053-1591/ab8dcf>.
- Ling, L.L., Liu, W.J., Zhang, S., Jiang, H., 2017. Magnesium oxide embedded nitrogen self-doped biochar composites: Fast and high-efficiency adsorption of heavy metals in an aqueous solution. *Environ. Sci. Technol.* 51, 10081–10089. <https://doi.org/10.1021/acs.est.7b02382>.
- Liu, P., Liu, W.J., Jiang, H., Chen, J.J., Li, W.W., Yu, H.Q., 2012. Modification of bio-char derived from fast pyrolysis of biomass and its application in removal of tetracycline from aqueous solution. *Bioresour. Technol.* 121, 235–240. <https://doi.org/10.1016/j.biortech.2012.06.085>.
- Liu, K., Li, H., Wang, Y., Gou, X., Duan, Y., 2015. Adsorption and removal of rhodamine B from aqueous solution by tannic acid

- functionalized graphene. *Colloids Surf. A* 477, 35–41. <https://doi.org/10.1016/j.colsurfa.2015.03.048>.
- Ma, C., Min, J., Gong, J., Liu, X., Mu, X., Chen, X., Tang, T., 2020. Transforming polystyrene waste into 3D hierarchically porous carbon for high-performance supercapacitors. *Chemosphere* 253, <https://doi.org/10.1016/j.chemosphere.2020.126755> 126755.
- Majd, M.M., Kordzadeh-Kermani, V., Ghalandari, V., Askari, A., Sillanpää, M., 2022. Adsorption isotherm models: A comprehensive and systematic review (2010–2020). *Sci. Total Environ.* 812, <https://doi.org/10.1016/j.scitotenv.2021.151334> 151334.
- Martins, A.C., Pezoti, O., Cazetta, A.L., Bedin, K.C., Yamazaki, D.A.S., Bandoch, G.F.G., Asefa, T., Visentainer, J.V., Almeida, V.C., 2015. Removal of tetracycline by NaOH-activated carbon produced from macadamia nut shells: Kinetic and equilibrium studies. *Chem. Eng. J.* 260, 291–299. <https://doi.org/10.1016/j.cej.2014.09.017>.
- Mosoarca, G., Vancea, C., Popa, S., Dan, M., Boran, S., 2022. The use of bilberry leaves (*vaccinium myrtillus* L.) as an efficient adsorbent for cationic dye removal from aqueous solutions. *Polymers* 14, <https://doi.org/10.3390/polym14050978>.
- Nekouei, F., Nekouei, S., Tyagi, I., Gupta, V.K., 2015. Kinetic, thermodynamic and isotherm studies for acid blue 129 removal from liquids using copper oxide nanoparticle-modified activated carbon as a novel adsorbent. *J. Mol. Liq.* 201, 124–133. <https://doi.org/10.1016/j.molliq.2014.09.027>.
- Omer, A.M., Dey, R., Eltaweil, A.S., Abd El-Monaem, E.M., Ziora, Z.M., 2022. Insights into recent advances of chitosan-based adsorbents for sustainable removal of heavy metals and anions. *Arab. J. Chem.* 15, <https://doi.org/10.1016/j.arabjc.2021.103543> 103543.
- Penafiel, M.E., Matesanz, J.M., Vanegas, E., Bermejo, D., Mosteo, R., Ormad, M.P., 2021. Comparative adsorption of ciprofloxacin on sugarcane bagasse from Ecuador and on commercial powdered activated carbon. *Sci. Total Environ.* 750, <https://doi.org/10.1016/j.scitotenv.2020.141498> 141498.
- Qiao, D., Li, Z., Duan, J., He, X., 2020. Adsorption and photocatalytic degradation mechanism of magnetic graphene oxide/ZnO nanocomposites for tetracycline contaminants. *Chem. Eng. J.* 400, <https://doi.org/10.1016/j.cej.2020.125952> 125952.
- Salaa, F., Bendenia, S., Lecomte-Nana, G.L., Khelifa, A., 2020. Enhanced removal of diclofenac by an organohalloysite intercalated via a novel route: Performance and mechanism. *Chem. Eng. J.* 396, <https://doi.org/10.1016/j.cej.2020.125226> 125226.
- Shu, J., Wang, Z., Huang, Y., Huang, N., Ren, C., Zhang, W., 2015. Adsorption removal of Congo red from aqueous solution by polyhedral Cu<sub>2</sub>O nanoparticles: Kinetics, isotherms, thermodynamics and mechanism analysis. *J. Alloy. Compd.* 633, 338–346. <https://doi.org/10.1016/j.jallcom.2015.02.048>.
- Su, C., Guo, Y., Chen, H., Zou, J., Zeng, Z., Li, L., 2020. VOCs adsorption of resin-based activated carbon and bamboo char: Porous characterization and nitrogen-doped effect. *Colloid. Surface A* 601, <https://doi.org/10.1016/j.colsurfa.2020.124983> 124983.
- Taoufik, N., Elmchaouri, A., Anouar, F., Korili, S.A., Gil, A., 2019. Improvement of the adsorption properties of an activated carbon coated by titanium dioxide for the removal of emerging contaminants. *J. Water Process Eng.* 31, <https://doi.org/10.1016/j.jwpe.2019.100876> 100876.
- Tran, T.H., Le, A.H., Pham, T.H., Nguyen, D.T., Chang, S.W., Chung, W.J., Nguyen, D.D., 2020. Adsorption isotherms and kinetic modeling of methylene blue dye onto a carbonaceous hydrochar adsorbent derived from coffee husk waste. *Sci. Total Environ.* 725, <https://doi.org/10.1016/j.scitotenv.2020.138325> 138325.
- Vu, M.T., Chao, H.P., Trinh, T.V., Le, T.T., Lin, C.C., Tran, H.N., 2018. Removal of ammonium from groundwater using NaOH-treated activated carbon derived from corncob wastes: Batch and column experiments. *J. Clean. Prod.* 180, 560–570. <https://doi.org/10.1016/j.jclepro.2018.01.104>.
- Wang, J.C., Kaskel, S., 2012. KOH activation of carbon-based materials for energy storage. *J. Mater. Chem.* 22, 23710–23725. <https://doi.org/10.1039/C2JM34066F>.
- Wang, Z., Zhou, Q., Chen, S., Liang, D., Tang, S., Chen, H., Chen, G., Xia, Y., Zhang, B., 2020. Preparation of a quinoa straw-derived porous carbon material and a Fe<sub>3</sub>O<sub>4</sub>-contained composite material for removal of rhodamine B from water. *Mater. Res. Express* 7, <https://doi.org/10.1088/2053-1591/abd0a5> 125603.
- Xiao, W., Garba, Z.N., Sun, S., Lawan, I., Wang, L., Lin, M., Yuan, Z., 2020. Preparation and evaluation of an effective activated carbon from white sugar for the adsorption of rhodamine B dye. *J. Clean. Prod.* 253, <https://doi.org/10.1016/j.jclepro.2020.119989> 119989.
- Yan, K., Chen, W., He, X., Zhang, G., Xu, S., Wang, L., 2010. Responses of photosynthesis, lipid peroxidation and antioxidant system in leaves of *Quercus mongolica* to elevated O<sub>3</sub>. *Environ. Exp. Bot.* 69, 198–204. <https://doi.org/10.1016/j.envexpbot.2010.03.008>.
- Yu, H., Wang, T., Yu, L., Dai, W., Ma, N., Hu, X., Wang, Y., 2016. Remarkable adsorption capacity of Ni-doped magnolia-leaf-derived bioadsorbent for congo red. *J. Taiwan Inst. Chem. Eng.* 64, 279–284. <https://doi.org/10.1016/j.jtice.2016.04.008>.
- Zhang, D., Yin, J., Zhao, J., Zhu, H., Wang, C., 2015. Adsorption and removal of tetracycline from water by petroleum coke-derived highly porous activated carbon. *J. Environ. Chem. Eng.* 3, 1504–1512. <https://doi.org/10.1016/j.jece.2015.05.014>.
- Zhao, W.Y., Zhou, M., Yan, B., Sun, X., Liu, Y., Wang, Y., Xu, T., Zhang, Y., 2018. Waste conversion and resource recovery from wastewater by ion exchange membranes: State-of-the-art and perspective. *Ind. Eng. Chem. Res.* 57, 6025–6039. <https://doi.org/10.1021/acs.iecr.8b00519>.
- Zhao, S., Meng, Z., Fan, X., Jing, R., Yang, J., Shao, Y., Liu, X., Wu, M., Zhang, Q., Liu, A., 2020. Removal of heavy metals from soil by vermiculite supported layered double hydroxides with three-dimensional hierarchical structure. *Chem. Eng. J.* 390, <https://doi.org/10.1016/j.cej.2020.124554> 124554.
- Zhu, L., Wang, Y., He, T., You, L., Shen, X., 2016. Assessment of potential capability of water bamboo leaves on the adsorption removal efficiency of cationic dye from aqueous solutions. *J. Polym. Environ.* 24, 148–158. <https://doi.org/10.1007/s10924-016-0757-8>.